

The dynamics of granular flow in an hourglass

Christian T. Veje, P. Dimon

Abstract We present experimental investigations of flow in an hourglass with a slowly narrowing elongated stem. The primary concern is the interaction between grains and air. For large grains the flow is steady. For smaller grains we find a relaxation oscillation (ticking) due to the counterflow of air, as previously reported by Wu et al. [Phys. Rev. Lett. **71**, 1363 (1993)]. In addition, we find that the air/grain interface in the stem is either stationary or propagating depending on the average grain diameter. In particular, a propagating interface results in power-law relaxation, as opposed to exponential relaxation for a stationary interface. We present a simple model to explain this effect. We also investigate the long-time properties of the relaxation flow and find, contrary to expectations, that the relaxation time scale is remarkably constant. Finally, we subject the system to transverse vibrations of maximum acceleration Γ . Contrary to results for non-ticking flows, the average flow rate increases with Γ . Also, the relaxation period becomes shorter, probably due to the larger effective permeability induced by the vibrations.

Keywords Granular flows, hourglass experiment, jamming

1 Introduction

Although hourglasses have been used to measure time intervals since the middle ages [1], the physics of grain flow is still a complicated and poorly understood process

Received: 11 February 2000

C. T. Veje (✉), P. Dimon
Center for Chaos and Turbulence Studies,
The Niels Bohr Institute, Blegdamsvej 17,
DK-2100 Copenhagen Ø, Denmark

We greatly appreciate the assistance of S. Hørlück with the video system. We would like to thank F. B. Rasmussen for providing the capacitance bridge and S. R. Nagel and H. M. Jaeger for help on the design of the capacitive measuring device. We have had many helpful and stimulating discussions with R. P. Behringer, E. Clément, and K. J. Måløy. We would particularly like to thank K. J. Måløy for bringing the work on pressure diffusion to our attention. Finally, the authors would like to thank Statens Naturvidenskabelige Forskningsråd (Danish Research Council) for support. Also, CV greatly appreciates the support of The Leon Rosenfeld Scholarship Fund.

[2–5]. Traditionally, an hourglass consists of two glass ampoules, partly filled with grains, connected by a small hole in the stem. Typically, ballotini (small glass beads), sand, marble powder, and even crushed egg shells have been used as the granular material [1]. Recently, the hourglass has become a source of interest to the physics community as a convenient simple system to investigate granular flows [1, 6–10].

The flow of granular materials has been found to exhibit a wide range of different phenomena. In particular, density waves and shock waves are common in dry granular flows. Density patterns due to rupture zones as grains flow through hoppers have been observed using X-ray imaging [11–13]. Using similar geometries and techniques, Baxter et al. found density waves propagating both with and against the flow direction, depending on the opening angle of the hopper [14]. For two-dimensional funnel flow through very narrow outlets (3–10 grain diameters), shock waves have been found due to arching at the outlet [15–17]. Moreover, due to the monodispersity of the grains, shock waves were created at particular locations where the width of the funnel would perfectly accommodate a triangular packing of balls [17]. Apparently, the density waves were initiated by the intermittent jamming of balls similar to the arching at the outlet. Recently, Clément has pointed out that the propagation direction of the density waves in two-dimensional vertical pipes depends on the coefficient of restitution of the balls [18].

For hourglasses in which one or both chambers are closed (except for the outlet), air must flow from the lower chamber to the upper during grain flow. This means that the system becomes a two-phase flow with a coupling between the grain and air flow. Theoretically, this problem remains a large challenge, but by regarding the air flow as a Darcy flow, simple models for the flow behavior are possible [7]. For flow through pipes there is a tendency for the grains to form plugs which propagate as a result of mass transfer balanced by the air flow [19–22]. The propagation of the plugs was found to depend sensitively upon the allowed air flow [21]. In the same geometry, Nakahara and Isoda found similar results using either water or silicone oil as the interstitial fluid [23].

In this article, the flow of grains through a slowly narrowing elongated stem is examined using a specially designed hourglass. The emphasis of the experiment is on the air/grain interaction. Using different techniques, the mass flow, air pressure, and density fluctuations are measured to form an overall picture of the dynamics of the flow.

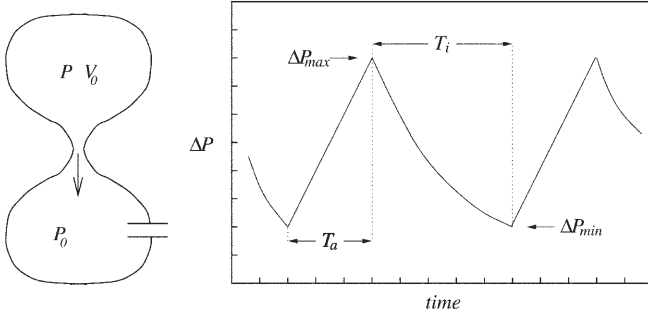


Fig. 1. Left: Schematic drawing of an hourglass. Right: Schematic representation of the pressure difference $\Delta P = P_0 - P$ between the upper chamber and the laboratory pressure as a function of time. The active and inactive times are indicated by T_a and T_i respectively

2 Flow in hourglasses

A schematic drawing of an hourglass is shown in Fig. 1 (left). For closed hourglasses, fluctuations in the grain density in the stem have been found to be quite reminiscent of the plugs observed in pipes [9]. This results in a non-steady flow as first studied by Schick and Verveen [6] using a light transmission technique. They claimed that the density fluctuations had a $1/f$ noise power spectrum, but it has been argued that this can be explained as a crossover region between characteristic time scales [10].

In 1993 Wu et al. reported on the ticking phenomenon of hourglasses [7]. They used an hourglass with a large opening half-angle $\beta = 45^\circ$ which makes the stem relatively short. For a minimum outlet width D and grain diameter d , they found that for small grains ($D/d > 12$) the flow exhibited a distinct periodic ticking. They argued that the ticking was due to the counterflow of air created by the outflowing grains. They identified an active phase with grain flow and an inactive phase with no grain flow. Fig. 1 (right) shows the qualitative time evolution of the pressure difference $\Delta P = P_0 - P$ between the pressure in the upper chamber P and the laboratory pressure P_0 . In the active phase, characterized by the active time T_a , the grain flow is sufficiently fast that air cannot flow back through the grains quickly enough to maintain equilibrium in the upper chamber, resulting in an under-pressure. Eventually, the pressure difference reaches a value ΔP_{max} large enough to stabilize an air/grain interface in the stem and the flow stops. Now the inactive phase begins and air flows back through the now stationary grain packing for an inactive time T_i . Once the pressure difference reaches a certain minimum value ΔP_{min} , it can no longer support the interface and the grains start to flow again.

We now reproduce the argument of Wu et al. [7] for the behavior of the inactive phase since we will need to modify it later. Consider an hourglass with an upper chamber of volume V_0 , partly filled with grains (see also Fig. 1). The chamber is closed so air can only leave or enter through the outlet of radius $R = D/2$. The bottom chamber is open to the atmosphere. Suppose a small mass of grains ΔM falls from the upper chamber in a relatively short time. Then the air volume V_a in the upper chamber expands leading to a small decrease in the air density Δn . It is assumed

that the air is an ideal gas so that $\Delta P = \Delta n k_B T$ where k_B is the Boltzmann constant and T is the temperature, and that the process is isothermal, hence, T is constant.

At the end of the active phase the flow stops when the pressure difference is large enough to stabilize the air/grain interface in the stem. Now the inactive phase begins. Air leaks through the porous packing of grains and the pressure slowly increases in the upper chamber. From the ideal gas law, we have

$$\frac{d\Delta P}{dt} = k_B T \frac{d\Delta n}{dt} . \quad (1)$$

Assuming that the air flow in the stem is incompressible, which is valid for the length and time scales involved here, the change in density Δn is related to the air volume flow rate q by

$$\frac{d\Delta n}{dt} = \frac{n_0 q}{V_a} \quad (2)$$

where n_0 is the air density at laboratory pressure. Combining Eqs. (1) and (2), we have

$$\frac{d\Delta P}{dt} = \frac{P_0}{V_a} q \quad (3)$$

where $P_0 = n_0 k_B T$ is the laboratory pressure. The air flow rate q is given by the Darcy equation

$$q = \pi R^2 \bar{v}_{air} = -\frac{\kappa \pi R^2}{\eta L} \Delta P \quad (4)$$

where \bar{v}_{air} is the average air velocity outside the grain packing, κ is the permeability, and L is a characteristic length over which the pressure difference ΔP occurs. Using Eqs. (3) and (4), we find

$$\frac{d\Delta P}{dt} = -\frac{\pi P_0 \kappa R^2}{\eta V_a L} \Delta P . \quad (5)$$

We write the solution as

$$\Delta P(t) = \Delta P_{max} e^{-t/\tau} \quad (6)$$

where

$$\tau = \frac{\eta V_a L}{\pi P_0 \kappa R^2} \quad (7)$$

is the characteristic decay time, and ΔP_{max} is the pressure needed to stabilize the air/grain interface from a moving packing. These are the results found by Wu et al. [7].

To estimate the minimum pressure difference ΔP_{min} needed to sustain a stable interface, we calculate the forces acting on a single grain sitting at the air/grain interface. First, of course, there is gravity

$$F_g = -mg \quad (8)$$

where m is the mass of a grain, and g is the gravitational acceleration. If we assume that the pressure gradient in the stem is approximately linear, then the gradient across a single grain results in a buoyancy force

$$F_b = \frac{\pi d^3}{6L} \Delta P . \quad (9)$$

Finally, there is the viscous drag on a grain from the air flow. We will assume that this is given by the Stokes law $F_d = 3\pi\eta d\bar{v}_{air}$, but since this is not a free grain, it should

be regarded as a rough approximation. It is, however, an interface grain so using \bar{v}_{air} from Eq. (4) makes sense since we are outside the bulk grain packing (note that κ is in fact defined through Eq. (4)). Thus, we write the dragforce as

$$F_d = \frac{3\pi\kappa d}{L} \Delta P . \quad (10)$$

Force balance requires that $F_g + F_b + F_d = 0$, from which we find the minimum pressure difference

$$\Delta P_{min} = \frac{mgL}{\pi d(3\kappa + d^2/6)} . \quad (11)$$

It should be noted that for the actual values used here, the relative size of the terms in the denominator is $3\kappa/(d^2/6) \sim 10^{-2}$ so F_d is, in fact, not that important at least during relaxation.

For similar types of hourglasses, Pennec et al. found that the slight curvature of the stem would actually create a small air bubble and a grain plug during the flow [9]. They also found that the plug oscillated, briefly causing the pressure in the upper chamber to oscillate during the active phase. Hence, the notion of a stationary interface is a special case only found for large opening angle geometries or small enough grain sizes. However, the effect of the geometry of the stem has largely been unexplored. Thus, a much more common scenario is the formation of plugs and bubbles, including oscillating and propagating interfaces, in the stem of an hourglass. These phenomena may be the origins of the instabilities observed in pipe flows, although in a very short-lived state. Pipe flow may therefore be considered as an extreme case of ticking with a non-stationary air/grain interface. The region between pipe flow (long stem) and stationary ticking (short stem) is the concern of this paper.

3 The experimental setup

A variety of grains have been used in this work, and are listed in Table 1. The ratio D/d determines the flow behavior discussed in section 2. We have primarily used grains of smooth glass beads (A7–A30). The A10 grains will be used as the reference grain type. The glass beads are produced in weakly polydisperse mixtures. The polydispersity is a skewed distribution with an average grain diameter d , with about 80% of the grains in the larger half of the size range. The R1 grains are crushed glass but still very compact and with sharp edges. An often cited type of

Table 1. The grain types that were used in the experiments. The diameter of the narrowest point of the outlet is $D = 0.3$ cm. The average grain diameter d is estimated from the size distribution

Type	Material	Range (μm)	d (μm)	D/d
A7	Smooth glass	70–110	~ 100	30
A10	Smooth glass	100–200	~ 180	18
A15	Smooth glass	150–250	~ 230	13
A30	Smooth glass	300–400	~ 380	8
R1	Crushed glass	200–500	~ 400	8
Boom	Rough sand	~ 200 –500	~ 250	12

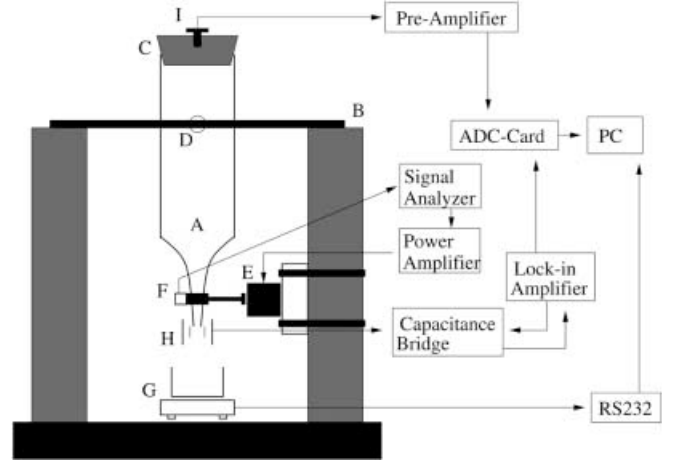


Fig. 2. Schematic of the experimental setup including the measuring devices described in the text

sand is the Booming Dunes sand (Boom). They are quite rough like the R1 grains but we have no nominal values for the size distribution.

A schematic drawing of the hourglass experiment is shown in Fig. 2. It consists of a glass cylinder reservoir (A) of length 35 cm and inner diameter 6 cm leading into a 15 cm long slowly narrowing stem. The smallest inner diameter $D = 0.3$ cm of the stem was at the outlet. The hourglass was supported by a frame (B) and placed on a heavy iron plate. The counterflow of air could be turned on and off by inserting a cork in the top of the reservoir (C).

The volume of the reservoir was $V_0 \sim 1000 \text{ cm}^3$ so with average mass flow rates varying from 0.1 to 3 g/s, typical runs lasted 10–100 minutes. For the smallest grains, changes in the humidity were found to seriously affect the flow. Thus, the humidity was monitored with a Dickson TH550 hygrometer and recorded for future reference. Measurements were only made when the humidity was between 30–50%.

The hourglass was mounted so that it could rotate freely about an axis (D). A Brüel & Kjær Mini-Shaker Type 4810 (E) was mounted on a wood plate attached to the frame. A brass rod was connected from the vibrator to the stem of the hourglass. The rod was fabricated in one piece so that there were as few joints as possible. The vibrator was driven by a power amplifier designed to operate as low as 1 Hz. The amplifier boosted a sine source from an HP3562A Dynamical Signal Analyzer (DSA). A Brüel & Kjær Cubic Delta-Tron Accelerometer Type 4503 was mounted on the rod, opposite the vibrator (F). The accelerometer has a calibrated output of 8.90 mV/g ($g = 9.82 \text{ m/s}^2$) for easy measure of the dimensionless maximum acceleration $\Gamma = A\omega^2/g$, where A is the amplitude and ω is the angular frequency of the vibration. The output from the accelerometer was measured by the DSA for a direct measure of the amplitude of vibration.

Several measuring devices were used. These are described below in more detail and include a scale for measuring the total mass flow (G), a capacitive flow detector (H), and a pressure gauge inserted in the reservoir (I). The video equipment to be described later is not shown.

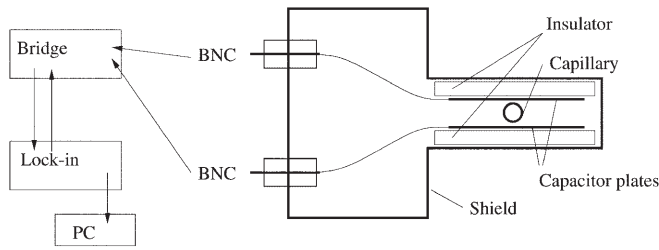


Fig. 3. Schematic top view of the capacitance measuring device

The total mass flow $M(t)$ was measured with a Sartorius PT1500 scale (range 0–1500 g, precision 0.1 g) placed under the outlet. The scale was connected to a PC through an RS-232 interface (5 Hz sampling rate). The relaxation time constant for the scale is ~ 1 s so the real-time resolution of the measurements is actually longer than the 0.2 s sampling time.

To obtain better time resolution of the flow rate fluctuations, a capacitive device was used in conjunction with a capacitance bridge. A schematic top view is shown in Fig. 3. The capacitor was aligned just below the outlet so the grain flow passed through its center. The black circle indicates the position of the stem outlet. The plates were separated by 1 cm and had dimensions of 1 cm by 4 cm. The capacitance with only air between the plates is ~ 0.5 pF. (The large dimensions of the capacitor plates were needed to make room for the horizontal vibration of the stem.) When sand passes through the capacitor, its capacitance C changes by an amount ΔC roughly proportional to the quantity of sand between the plates. For example, using the known polarization for a sphere in a constant electric field, with a diameter much smaller than the distance between the capacitor plates, it is found that

$$\frac{\Delta C}{C} = \left[1 - \left(\frac{3}{K+2} \right)^2 \right] \frac{V_g}{V_c} \quad (12)$$

where V_c and V_g are the volume of the capacitor and a single grain, respectively, and K is the dielectric constant of the grain material. For glass, $K \sim 5$, so for a grain diameter $d = 0.018$ cm, Eq. (12) yields $\Delta C \sim 6 \cdot 10^{-7}$ pF for a single grain between the plates.

The capacitor was shielded by a metal cage to avoid external noise. It was connected to a General Radio 1615-A Capacitance Bridge which can be balanced to within $\sim 10^{-5}$ pF. With this resolution, we can detect ~ 100 grains. The bridge was driven by a Stanford Research SR810 lock-in amplifier at 60 kHz with an amplitude of 5 V. The bridge was always nulled with no grains present. To ensure that the lock-in did not overload during flow, grains were first poured through the hourglass without inserting the cork which gives the maximum possible flow and hence the maximum capacitance change ΔC . The output from the lock-in amplifier was recorded at 50 Hz by an ADC card in the PC. The time constant on the lock-in amplifier was set to 30 ms (24 dB rolloff) to serve as a Nyquist filter.

The pressure in the reservoir was measured with an Omega PX170 differential pressure transducer (range 0–0.38 Bar) inserted in a hole in the cork. The nominal

response time of the transducer is ~ 1 ms which was more than adequate. The transducer was powered with a 9 V battery. Its output was amplified with a Stanford SR560 low-noise preamplifier and Nyquist filtered at 30 Hz with the amplifier's low-pass filter. The signal-to-noise ratio was $\sim 10^3$. Amplifying the signal by 100–1000 made it possible to easily distinguish pressure differences as small as 0.1 mBar. However, the internal bridge in the transducer has as low an accuracy as 0.5 mBar in the nulling, leading to a systematic error in the value of the pressure difference. The output from the amplifier was also read by the ADC card, simultaneously with the capacitance measurements. This made it possible to completely synchronize the capacitance and the reservoir pressure.

For visualization purposes, and in order to quantitatively track the air/grain interface in the stem, a video measuring system developed for another experiment was also used. It is summarized here but discussed in detail elsewhere [17].

The camera was a Pulnix TM-6701AN, 8-bit gray scale, non-interlaced analog CCD camera. The resolution was 640 by 480 pixels. It was placed about 50 cm from the stem with a black background for contrast. A halogen light source behind the camera gave the sand a bright appearance. Dark areas have little or no sand. Consecutive images were taken at 60 frames/s. The analog output was read by a Matrix Vision PCimage SGVS frame grabber card for easy storage on a PC. Fig. 4 shows a sequence of frames during flow of A10 grains. An air/grain interface can be seen propagating upwards. In frame number 180 the interface collapses. This sequence only lasts little more than one second, whereas the entire relaxation cycle takes about 6 s. After the collapse, an air bubble is formed with an initial length of ~ 3 cm which then gradually shrinks while the air pressure equilibrates through the grain packing.

Using films like these, only up to 3 s of data could be recorded. To increase the measuring time, individual frames were averaged horizontally to give a one-dimensional sequence of the mean grain density at a given height

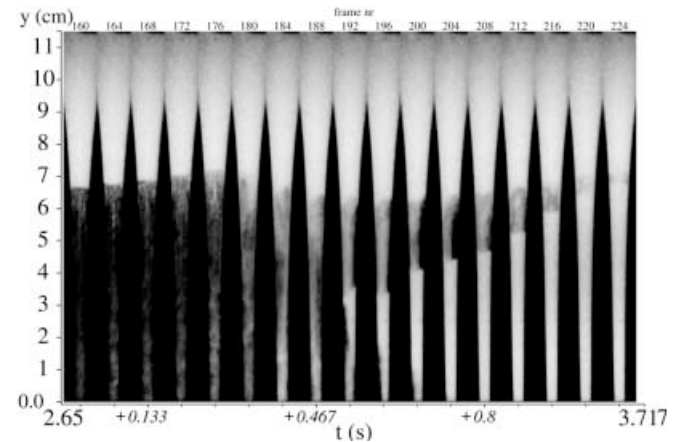


Fig. 4. Short film sequence showing the collapse of an interface and the accompanying creation of an air bubble. The grains are type A10. (The width of the stem becomes larger than the width of the frames at $y \sim 9.5$ cm.)

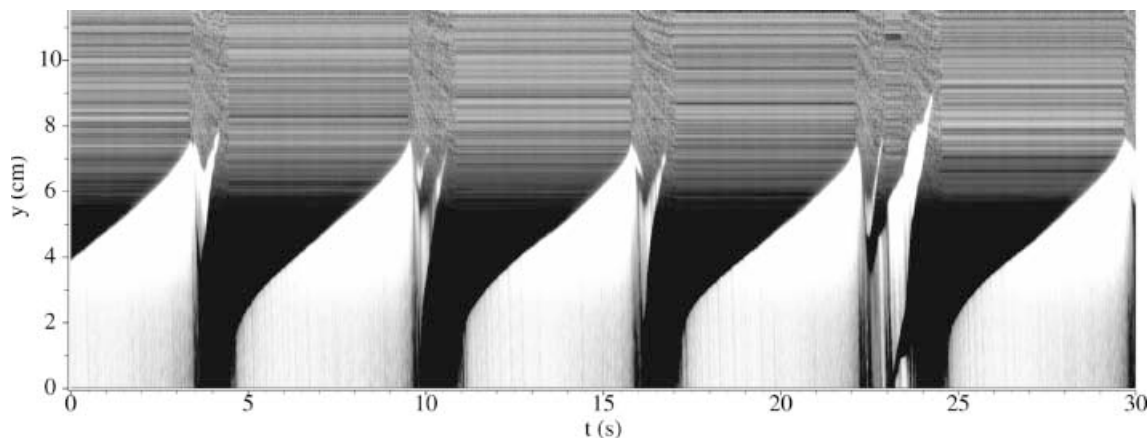


Fig. 5. Example of an averaged space–time density map (in reverse video) of periodically relaxing flow using A10 grains.

y in the stem. Now measurements up to 7 minutes could be taken.

An example of such a density space–time diagram is shown in Fig. 5 in reverse video also using A10 grains. The gray scale in the figure is a relative measure of the light intensity at a given height. The outlet of the stem is at $y = 0$ and the bright regions at the bottom reflect low grain density. Higher up, bright areas only reflect the current deviation from a certain mean gray-scale value. The bright and dark features for large y are not density fluctuations but merely fluctuations in the reflected intensity from the grain packing. The horizontal lines thus indicates that these grains are not moving. An electronic time stamp was used to synchronize the pressure signal with the video sequence, and hence, with the motion of the air/grain interface.

Before measuring, the hourglass was cleaned and the grains were poured through a large mesh sieve to eliminate impurities or clumping caused by humidity. Once a flow was initiated, after a small transient time (about 3–4 relaxations), measurements could begin. Measurements were made in two different combinations. In the first, the pressure difference ΔP , capacitance change ΔC , and mass flow $M(t)$ were measured simultaneously. The first two were synchronized, while the third had a time lag of about 2–3 s since it was measured using a different software program. In the second, the pressure difference and video measurements were taken together, and synchronized using the time stamp.

4 Relaxation oscillations and the air/grain interface

A common feature of all the grains found in Table 1 is that the flow is steady without ticking if the cork is not inserted. For the A30 grains this is also the case when the cork has been inserted. These grains are well out of the ticking regime described by Wu et al. [7], namely, $D/d \sim 8$, and smooth enough that the coupling between the air and grain flow is so weak that the flow finds a stable state where grains flow out and air flows in without causing significant density fluctuations.

Bright areas therefore correspond to low grain density and vice versa. Horizontal lines indicate motionless grains

For the rest of the grains we find a variety of ticking or relaxation phenomena as described above. In the following some of these will be analyzed in detail and others merely presented to show the effects of slight changes in grain size and shape.

4.1 Propagating interfaces (A10 grains)

A density map of the flow using these grains was shown in Fig. 5. It can be seen that the flow has an almost periodic ticking with a period of 5–6 s. Grains leave the stem at the outlet ($y = 0$) cm for 1–2 s (the active phase) after which an air/grain interface is created at about $y = 2$ cm due to the counterflow of air. At this point grains above the interface stop moving as indicated by the horizontal lines in the top part of the stem (see Fig. 5). The flow is now in the inactive phase. However, the interface, although well-defined, is no longer stationary. Grains are continuously falling out from the interface, causing it to propagate up through the stem. The movement of the interface and the mass flow are then directly related through the geometry of the stem.

When the interface reaches a point $y_{max} \sim 7$ cm, the air flow and buoyancy forces in the grains can no longer sustain the interface. The interface collapses and the flow enters the active phase again. Note that during the collapse, or the active phase, a bubble is formed which propagates, first down and then up through the grain packing (see also Fig. 4). During upward propagation, the vertical extent of the bubble diminishes as air leaks through the packing.

Fig. 6 shows the simultaneous measurements of pressure and capacitance (a), and mass flow (b). The pressure shows the expected qualitative behavior discussed in section 2. There is a fast time scale corresponding to the active period and a longer relaxation time in the inactive period. During the slow relaxation, the pressure difference decreases, but not in the exponential manner expected from the discussion in section 2. We will return to this point later. The capacitance shows that the flow occurs continuously during the active period. We see that the

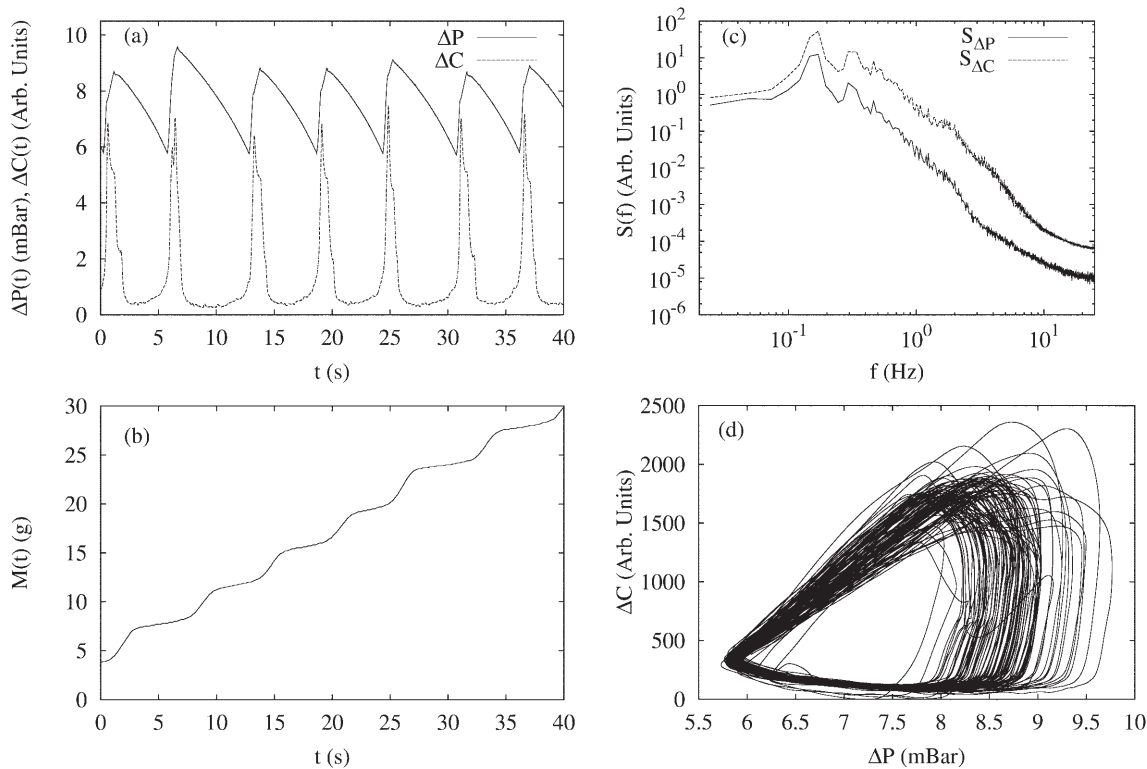


Fig. 6. **a** The pressure difference, capacitance change and **b** total mass flow versus time for A10 grains. **c** The power spectra

of the pressure and capacitance signals. **d** A parametric representation of the pressure and capacitance signals

maximum flow rate is reached just before the maximum pressure difference.

The power spectra $S_{\Delta P}(f)$ and $S_{\Delta C}(f)$ of the pressure and capacitance signals, respectively, are shown in Fig. 6(c). The peaks represent the period of the ticking. They also have a significant width, corresponding to a coherence time of about 20 s. Both the second and third harmonics can also be seen in the spectra, with amplitudes decaying as f^{-2} arising from the discontinuities in the signal. At about 1 Hz there is a small shoulder corresponding to the fast rise time of ~ 1 s in the active period which can be seen in the time signals Fig. 6(a).

A parametric plot of the capacitance vs. pressure is shown in Fig. 6(d). The long time scale during the inactive phase is at the bottom of the plot. The pressure slowly decreases with an almost constant flow rate. When the interface collapses, the flow rate increases dramatically while the pressure increases. When the pressure reaches ΔP_{max} , the interface forms, the flow rate drops dramatically, and the cycle repeats. An interesting question is if there is a correlation between values of the pressure extrema. We have checked for this by using both a Lomb periodogram and directly computed power spectra and found that there were no significant correlations.

4.2 Stationary interfaces (A7 grains)

We now turn to the smallest grains (type A7), which is well in the ticking regime ($D/d \sim 30$). Fig. 7 shows the

density map for this flow. We see that there is a stable stationary interface close to the outlet. The interface breaks up in more or less regular intervals of ~ 5 s, letting out lumps of grains, after which it stabilizes again at a new position. Note that the ejection of these lumps of grains does not contribute to movement of the rest of the grains in the stem. At certain points the interface collapses and the entire column of grains flows downwards after which the interface stabilizes at a new position close to the outlet.

Fig. 8(a) shows the simultaneous measurements of the pressure and capacitance. We see a dramatic increase in ΔP as the interface collapses, accompanied by a burst of outflowing grains visible in the capacitance signal. After such a collapse, the pressure relaxes through the porous packing in the stem. The intermittent ejection of small lumps of grains does not contribute to movement of the rest of the grains in the stem so the pressure continues to relax. A small kink in the pressure signal can be observed and is due to the decrease in the length L over which the pressure decays. When a lump of grains falls, L becomes slightly smaller.

This means that the balance pressure also becomes smaller and the pressure can continue relaxing until it reaches the new value of ΔP_{min} . Once the pressure reaches the minimum pressure the whole column of grains collapses and the stem refills. Thus there is an extra time scale involved concerning the intermittent ejection of small lumps of grains. The power spectra of the pressure signal in Fig. 8 shows a peak at about 0.075 Hz corresponding to a period of about 13 s.

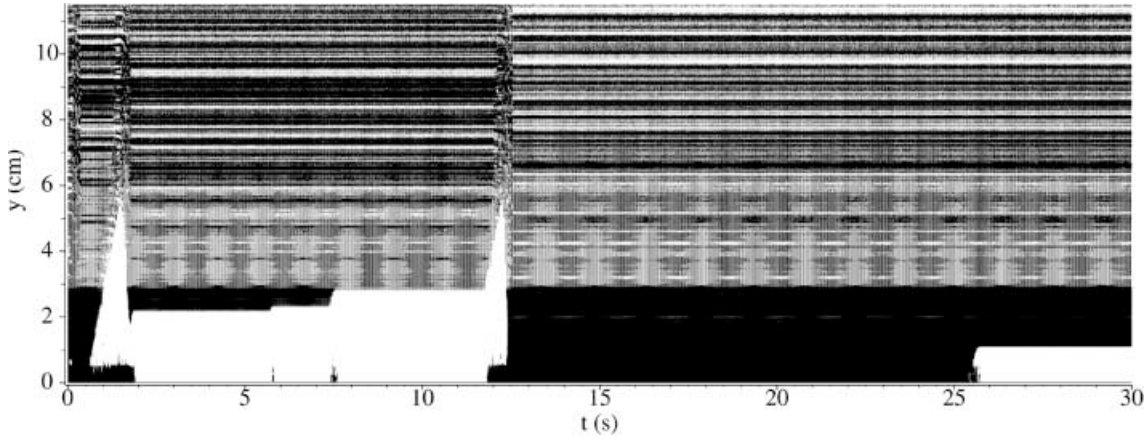


Fig. 7. Space-time density plot for A7 grains

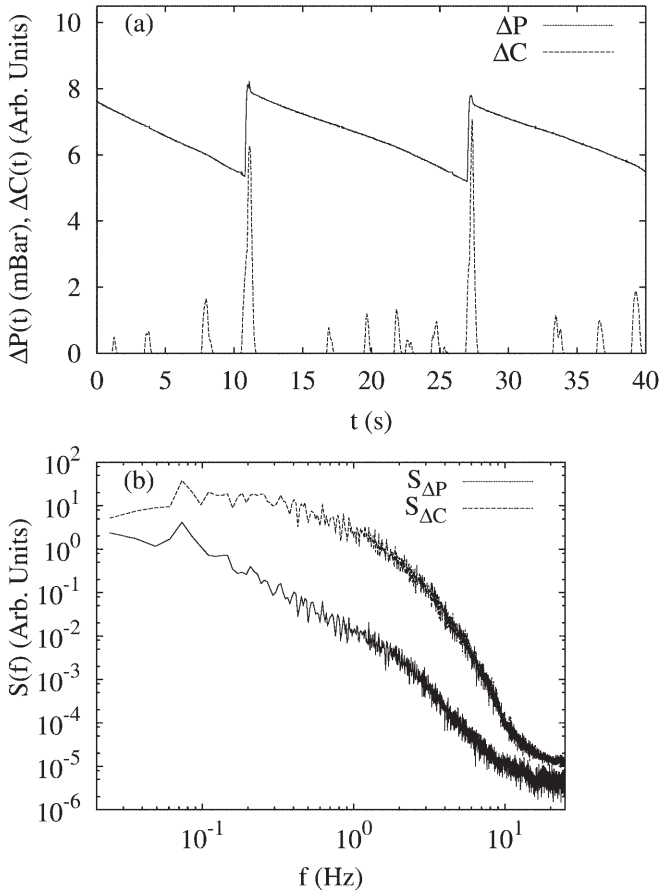


Fig. 8. **a** Signals of the pressure and capacitance versus time for grain type A7. **b** The power spectra of the pressure and capacitance signals

4.3 Edge detection and pressure decay

We now return to the A10 grains and the non-exponential pressure decay. Using an edge detection technique on the density map (Fig. 5), we can track the air/grain interface as it propagates up through the stem. The technique simply detects the point with the largest gradient in the density and uses that as the location of the interface. Since

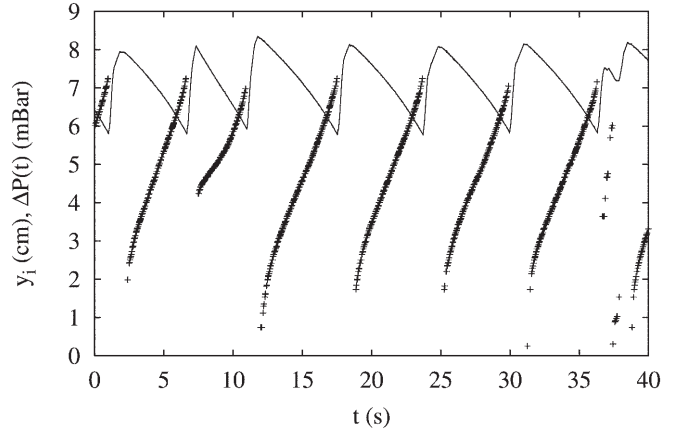


Fig. 9. The position y_i of the interface (points) and the simultaneous pressure difference (lines) versus time for A10 grains. The gaps in y_i occur during the active phase when the air/grain interface is not well-defined

the interface is largely undefined during the active periods, the tracking technique does not return any data for this period.

The position of the edge y_i and the simultaneous pressure difference is shown in Fig. 9. Clearly the decay of the pressure is not exponential as argued for stationary ticking in section 2 and as discussed in section 4.1. The departure from pure exponential relaxation may be primarily attributed to the change in the length L over which the pressure difference decays. Less importantly, the change in the stem diameter may also cause deviations from exponential.

These effects can be incorporated into the theory in section 2, but let us first consider the effect of the grains in the reservoir on the pressure drop. We will use a simplified model of an hourglass regarding it as two pipes connected in series as shown schematically in Fig. 10 (left). The measured pressure difference is the sum of the pressure drops in each pipe, i.e., $\Delta P = \Delta P_1 + \Delta P_2$. Since we assume that the flow is incompressible, the flow rate q is conserved, hence, using Eq. (4), we have

$$\frac{R_1^2 \kappa_1}{L_1} \Delta P_1 = \frac{R_2^2 \kappa_2}{L_2} \Delta P_2 . \quad (13)$$

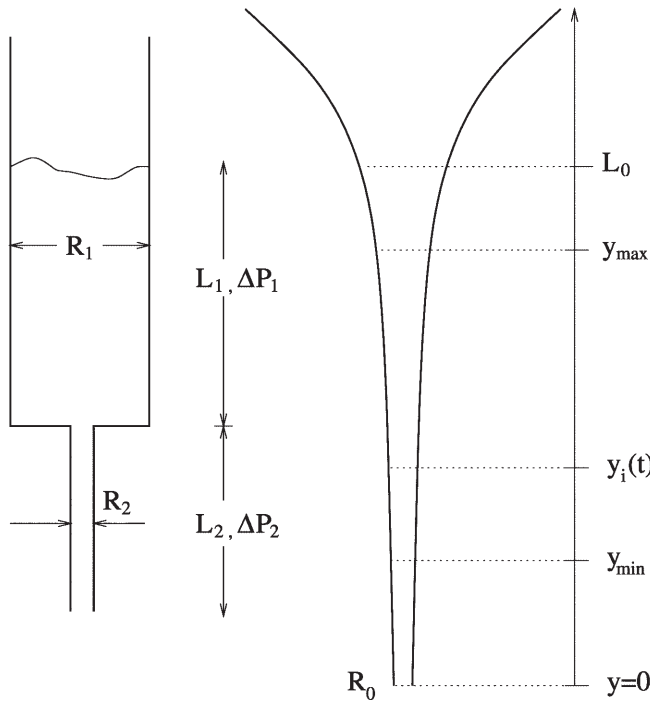


Fig. 10. Left: Two-pipe model of the hourglass (see text). Right: Different coordinates used for the relaxation model (see text)

If the pipes are *not* filled with grains, then for circular pipes $\kappa_{1,2} = R_{1,2}^2/8$. In this case the pressure drop in the the reservoir is given by

$$\frac{\Delta P_1}{\Delta P_2} = \frac{L_1}{L_2} \left(\frac{R_2}{R_1} \right)^4. \quad (14)$$

Thus, if $L_1 \sim L_2$ and $R_1 \sim 10R_2$, then $\Delta P_1 \ll \Delta P_2$. However, if the pipes are filled with grains, then the situation changes. In this case, the permeability only depends on the grain size which is the same in both pipes. Thus, $\kappa_1 = \kappa_2$ and Eq. (14) becomes

$$\frac{\Delta P_1}{\Delta P_2} = \frac{L_1}{L_2} \left(\frac{R_2}{R_1} \right)^2. \quad (15)$$

This ratio is not as small as it was in Eq. (14), but even in this case, $\Delta P_1/\Delta P_2 \sim 1\%$ so for the rest of the discussion we take $\Delta P = \Delta P_2$.

Although R is not constant, its dependence on y is so weak that we will assume $R = R_0$. Thus, the pressure still obeys Eq. (5) but in the more general form

$$\frac{d\Delta P}{dt} = -\frac{\pi P_0 \kappa R_0^2}{\eta V_a L(t)} \Delta P \quad (16)$$

where $L(t)$ now depends on time. The coordinates used in the model are indicated in Fig. 10 (right). We assume (from Fig. 9) that the propagation of the interface is a linear function of time

$$y_i(t) = y_{min} + v_0 t \quad (17)$$

where the interface velocity v_0 and starting point y_{min} are determined from the interface tracking data.

Hence, $L(t) = L_0 - y_i(t)$ where L_0 is the characteristic length over which the pressure decays when the stem is full (see Fig. 10). Then, using Eq. (17), Eq. (16) becomes

$$\frac{d\Delta P}{dt} = -\frac{\pi P_0 \kappa R_0^2}{\eta V_a (L_0 - y_{min} - v_0 t)} \Delta P. \quad (18)$$

We now define the relaxation time as (compare with Eq. (7))

$$\tau = \frac{\eta V_a (L_0 - y_{min})}{\pi P_0 \kappa R_0^2} \quad (19)$$

and write Eq. (18) as

$$\frac{d\Delta P}{dt} = -\frac{1}{\tau} \frac{\Delta P}{(1 - t/\tau_0)} \quad (20)$$

where $\tau_0 = (L_0 - y_{min})/v_0$. Integration now yields

$$\Delta P(t) = \Delta P_{max} (1 - t/\tau_0)^{\tau_0/\tau} \quad (21)$$

where ΔP_{max} is the initial value of the pressure at the beginning of the inactive phase. Thus, as a consequence of the propagation of the interface, the pressure now decays algebraically. As $v_0 \rightarrow 0$ then $\tau_0 \rightarrow \infty$ and we correctly recover Eq. (6) for a stationary interface.

As stated earlier, the interface velocity v_0 is determined from the interface tracking data. Using the form Eq. (17), we extract a mean value $\langle v_0 \rangle = 1.00 \pm 0.06$ cm/s from a total of 48 relaxation cycles. The average value for y_{min} was $\langle y_{min} \rangle = 2.2 \pm 0.3$ cm which is consistent with Figs. 5 and 9. Using these values the validity of the model can be tested by fitting the pressure data. Fig. 11 (top) shows a fit to the pressure data for a single relaxation. The data is fitted to Eq. (21) with ΔP_{max} , τ_0 and τ as free parameters. Multiple fits were done to see if the fitted parameters were robust. Only decays which lasted longer than 4 s were included to eliminate fluctuations, such as small decays (like the one at about 38 s in Fig. 9). Fig. 11 (bottom) shows the values of the fitted parameters for 48 relaxations as a function of the starting time. The parameters are quite constant. The average values are: $\langle \Delta P_{max} \rangle = 8.1 \pm 0.2$ mBar, $\langle \tau_0 \rangle = 7.9 \pm 0.7$ s and $\langle \tau \rangle = 24 \pm 2$ s.

Using the result for $\langle v_0 \rangle$ and $\langle \tau_0 \rangle$ we estimate $\langle L_0 \rangle = \langle \tau_0 \rangle \langle v_0 \rangle + \langle y_{min} \rangle = 10.0 \pm 1.7$ cm. This is the point where the stem has become wide enough that the permeability of the stem and grain packing no longer plays a role, i.e., we are now in pipe 1 in Fig. 10 (left). This value is reasonable since the interface never reaches such a large y value.

A determination of τ from the constants which enter in Eq. (19) is not possible since the value of κ is not known precisely. Using the known constants, $\eta = 1.7 \cdot 10^{-4}$ g/cm s, $P_0 = 10^6$ dyn/cm² and $V_a = 500$ cm³, and the fitted values for $\langle \tau \rangle$ and $\langle L_0 \rangle$, we obtain a value of $\kappa = (3.9 \pm 0.5) \cdot 10^{-7}$ cm², which is in reasonable agreement with the expected value for grains of this size [7].

As already shown, the pressure dynamics for the A7 grains are quite different from the A10 grains. As shown in Fig. 8 and Fig. 11 (top) the pressure decay has a curvature opposite to that of the A10 grains. Since in this case the interface is stationary, we use Eq. (6). In Fig. 11 (top) the pressure decay during a single relaxation is shown. Fitting the data to Eq. (6) with ΔP_{max} and τ as free parameters,

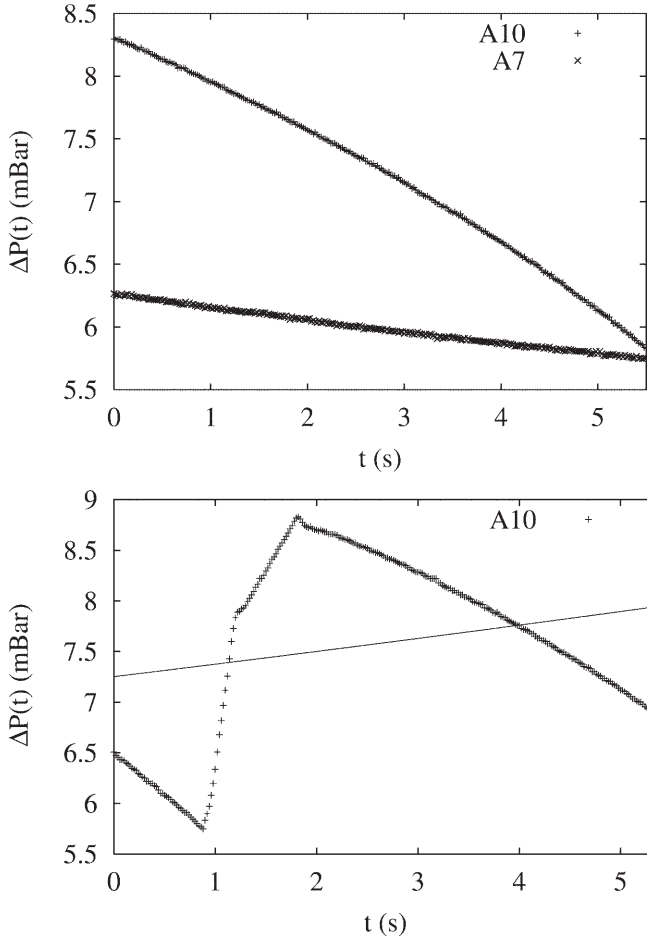


Fig. 11. Top: The measured pressure decay in a single relaxation cycle for grain types A7 and A10. The solid lines are fits using Eqs. (6) and (21) for A7 and A10 respectively. Bottom: By repeating the procedure in the top figure, the fitted parameters for grain type A10 are obtained for a sequence of relaxation cycles (see text). Points are connected for clarity

we obtain $\tau = 66.6 \pm 0.2$ s. This may again be related to the permeability κ through Eq. (7) resulting in a value $\kappa = (8 \pm 2) \cdot 10^{-8}$ cm² which is again within the expected range.

4.4 The oscillation mechanism

We now turn to the mechanism of the oscillation which in particular concerns ΔP_{min} and ΔP_{max} . Recall the arguments leading to Eq. (11) which expresses the minimum pressure difference needed to sustain a stable interface. Using the numbers found above, Eq. (11) yields the result $\Delta P_{min} \sim 5$ mBar which is very close to the value of ~ 6 mBar (seen from Fig. 6(a)) when the interface collapses. Recall that Eq. (11) was derived using only the mass of a single grain.

How can it be that grains can fall off the interface, causing it to propagate, when the grain packing is fully stabilized? Consider a grain placed in the packing during relaxation of the pressure. The force balance is given by Eq. (11). For grains outside the packing, however, the

pressure gradient is essentially zero since the pressure relaxes very fast when there is no grain packing giving a sufficient permeability. We will now consider again what happens to a grain sitting at the interface. The pressure gradient will relax over the grain diameter in a characteristic time τ_r . This will cause the buoyancy term Eq. (9) in the force balance to vanish. The balance equation for the interface grain then becomes

$$\Delta P_{int} = \frac{mgL(t)}{3\pi d\kappa} \quad (22)$$

If $\Delta P < \Delta P_{int}$ the grain will fall. On the other hand if $\Delta P < \Delta P_{min}$ the grain packing will collapse. Thus we have a range for ΔP

$$\Delta P_{min} < \Delta P < \Delta P_{int} \quad (23)$$

in which the packing is stable but the interface will propagate. If $\Delta P > \Delta P_{int}$ the interface is stationary. Of course all these values depend on time and as ΔP decays the collapse criterion $\Delta P < \Delta P_{min}$ is eventually reached.

The characteristic time τ_r essentially determines the velocity of the interface through $v_0 = d/\tau_r$. The velocity v_0 is known from the edge analysis. Since $\tau_r \sim d/\bar{v}_{air}$ we have that $v_0 = \bar{v}_{air}$ which we may estimate during a pressure relaxation. Using Eq. (4) we obtain $\bar{v}_{air} \sim 2$ cm/s which is indeed comparable to the velocity of the interface. This gives a relaxation time $\tau_r \sim 9$ ms.

As the interface collapses, the packing dilates resulting in a larger permeability and thus a larger ΔP_{min} . Now the grains start flowing from the reservoir and ΔP increases until it reaches the new ΔP_{min} . Then an interface is formed close to the outlet and grains from above settle on the newly formed packing. This is where the air bubble shown in Fig. 4 becomes trapped. While the air bubble decays, the pressure difference continues to increase, only now at a different rate. This can be seen by close inspection of the pressure signal in Fig. 9. During the active period ΔP increases, quickly at first until the bubble is formed, and then slightly slower while the bubble decays.

4.5 Results for other grain sizes and shapes

One of the most important parameters determining the flow behavior is the properties of the grains. The size and shape are especially important. In Fig. 12a–c we show the density maps for grain types A15 (a), Booming sand (b) and rough grains (c). Comparing with Figs. 5 and 7, we see that the different grains show quite a diversity of flow patterns.

For the larger grains, A15 and Booming sand, the scenario with the propagating interface is still pronounced. The relaxation time is faster due to the larger permeability of the packing. For R1 grains the active periods completely dominate the flow. The flow is interrupted at regular intervals by inactive bursts as an interface is briefly created. This causes a short decrease in the pressure and flow rate, but since the grains are rough and the permeability high, the interface breaks down very fast.

Thus it may be argued that when the permeability of the grain packing increases, that is, when the grain size increases, the relaxation time becomes shorter. At some

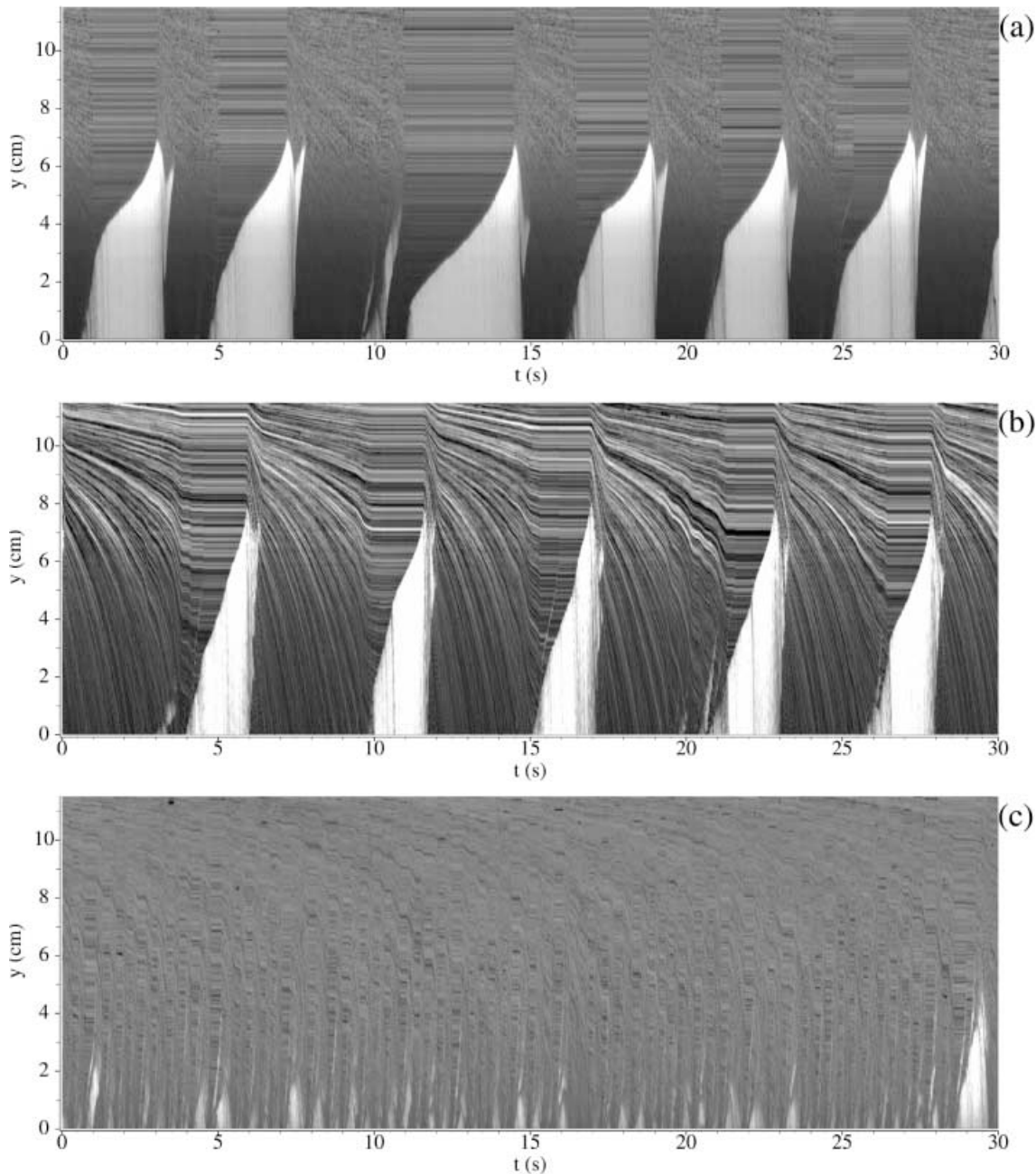


Fig. 12a–c. Space–time density plots for different grain types: **a** A15, **b** Boom and **c** Rough grains (R1)

point the permeability becomes large enough that the ticking completely vanishes. This happens for the type A30 grains where the flow is continuous with no relaxation effects. This result agrees well with the discussion in section 2 since $D/d \sim 8$ and is now out of the ticking range. For even larger grains ($d \sim 700 \mu\text{m}$) mechanically stable arches form in the stem and the flow stops completely.

Considering the similarity between the two grain types R1 and Booming sand, it is quite interesting how they differ in flow behavior. Figs. 12a–c (b) and (c) show there are fundamental differences in the relaxation process. This is striking since not only the size range but also the shape of the grains are very similar. An explanation is probably to be found in differences in density and of the friction

properties between real sand and glass. In fact, there are more similarities between the flow of the Booming sand and the A15 grains (Fig. 12a–c (a)) although the difference in average grain size is significant.

5 Non-stationary effects

In the above analysis it was assumed that the underlying process is stationary. However the process of emptying an hourglass is, in fact, inherently non-stationary. The characteristic relaxation time τ Eq. (7) includes the volume of air in the upper chamber V_a . Obviously V_a will slowly increase as grains flow out.

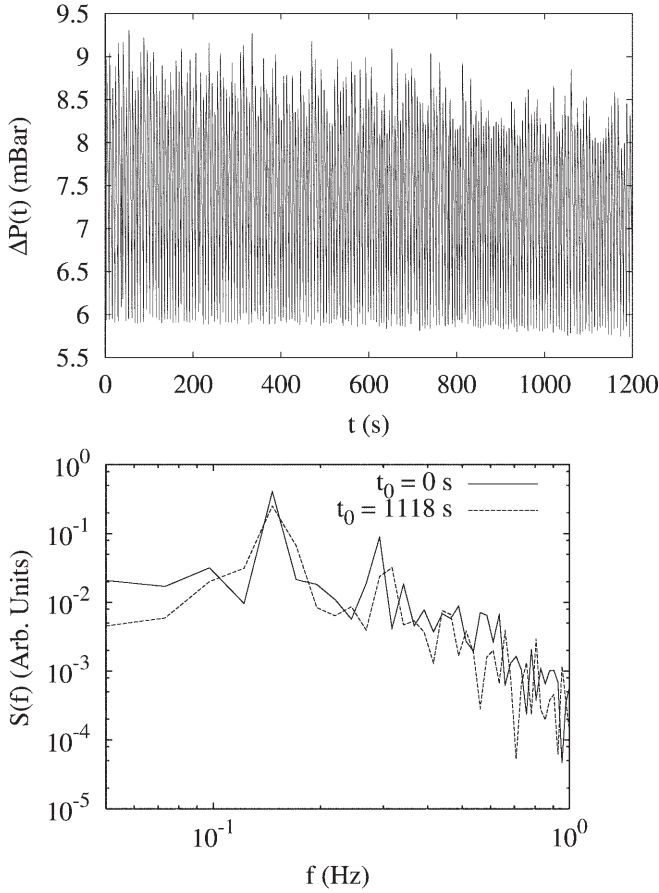


Fig. 13. Top: Pressure signal using A10 grains for the total time span from a full reservoir to an almost empty reservoir. Bottom: Power spectra of the pressure signal of ~ 80 s segments of the signal for different starting times t_0 (see text)

To investigate this non-stationary effect, the method is straightforward: fill the reservoir with grains and measure until it is empty. Since the average flow rate appears constant (see e.g. Fig. 6) one would expect the relaxation time τ , and therefore the ticking period to increase linearly with time following Eq. (7). However, this turned out not to be the case. In Fig. 13 (top) the pressure signal is shown for A10 grains. The time span is 1200 s which is nearly the time it takes to empty a full reservoir for this grain type. Clearly there are non-stationary signatures in the signal, in particular, the values of ΔP_{max} decrease with time.

As a first test of the non-stationarity, the power spectra of different segments of the pressure signal are considered in Fig. 13 (bottom). Taking the power spectra of the first and last 4096 points in the pressure signal, we obtain spectra for both a nearly full and nearly empty reservoir. We focus on the peaks of the spectra. If the relaxation period had significantly changed, the peak positions would have moved. Contrary to expectations, the peaks remain at the same frequency (within the resolution of the measurements).

Since $V_0 = V_a(t) + V_g(t)$ where $V_g(t)$ is the total volume of grains in the reservoir at time t , then assuming that the average flow rate of the grains Q is constant, we get

$$\frac{dV_a}{dt} = \frac{1}{\rho_m} \frac{dM}{dt} = \frac{Q}{\rho_m} . \quad (24)$$

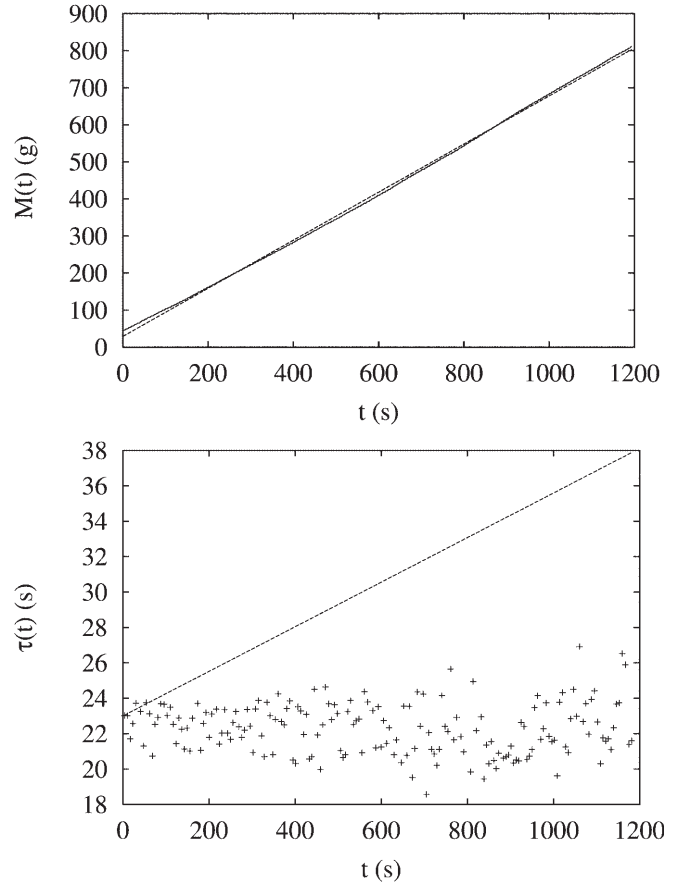


Fig. 14. Top: Mass on the scale as function of time. The dashed line is a linear fit. Bottom: The relaxation time τ as function of time. The data is obtained by fitting the pressure signal as described in section 4.3. The dashed line is the expected $\tau(t)$ from Eq. (25)

so that

$$\tau(t) = \frac{\eta(L_0 - y_{min})}{\rho_m P_0 \pi \kappa \langle R \rangle^2} Q t + \tau(0) . \quad (25)$$

The average flow rate Q is easily found by fitting the mass flow signal from the scale as shown in Fig. 14 (top). A value of $Q = 0.65$ g/s is obtained. In Fig. 14 (bottom), the relaxation time τ is shown for successive relaxations. The values have been fitted from the data in Fig. 13 (top) using the same method as in section 4.3. First we note, as we already knew, that τ has significant fluctuations. Second, we see that there is no linear increase as predicted. However, there is a weak tendency for the fluctuations to increase in time. Using the numbers from section 4.3 and the density $\rho_m = 2.5$ g/cm³, the prediction from Eq. (25) is also shown. It is remarkable how insensitive τ is to the change in V_a .

It has been suggested that an extra time scale concerning pressure diffusion may account for this unexpected result [24]. As argued by Penec et al. [25], there is a pressure diffusion constant D_P in a porous medium which gives rise to a characteristic time τ_P to form a pressure gradient. For a porous medium, this characteristic time is significantly longer than the time associated with the

speed of sound over the same distance. Following [25] we use $D_P \sim P_0 \kappa / \eta$ and so

$$\tau_P \sim \frac{L_0^2}{D_P} \sim \frac{\eta L_0^2}{P_0 \kappa}. \quad (26)$$

If τ_P were the slower time scale, i.e., if $\tau_P > \tau$, then it would dominate the relaxation process. Since it is independent of V_a (or any other time dependent parameter) this would explain the constancy of the relaxation time. However, the ratio

$$\frac{\tau_P}{\tau} = \frac{\pi R_0^2 L_0}{V_a} \quad (27)$$

is the ratio of the volume of the stem to the reservoir which is always small. Even for a full reservoir $V_a \sim V_0/2$ so $\tau_P/\tau \sim 10^{-3}$. Thus, this time scale cannot explain our results which still remain a mystery.

6 External excitation of the grain flow

Some experiments have been done on horizontally vibrated flows in hoppers [26,27]. Among other things, these experiments were concerned with the dependence of the average flow rate on the maximum acceleration. In Fig. 15 (top) we show results for the A7 type grains (see Table 1). The flow is steady since the cork is out. The

average flow rate Q decreases weakly as Γ increases. This result is attributed to the dilation effect due to the vibration. As the acceleration increases, the packing dilates and the mass flow thereby decreases.

Turning to the relaxation flow, the effects of vibrations on two different grain types are considered. The first is type A10 which had a propagating interface. The second is type A7 which had a stationary interface. As in chapter 4, the mass flow, pressure and capacitance were measured.

Contrary to the results for a steady flow, vibrations on a relaxing flow tend to increase the flow rate. This can be seen in Fig. 15 where the flow rate dependence on Γ for different frequencies is shown. Clearly there is a dependence on the driving frequency. Generally we may argue that the flow rate must increase since vibrations increase the permeability of the grain packing due to dilation effects.

The pressure and capacitance signal of the A10 grains for different values of Γ are shown in Fig. 16. The vibration frequency is $f = 30$ Hz. The relaxation flow becomes increasingly irregular as Γ is increased. For the largest values of Γ , periodic relaxation has almost disappeared. One can imagine that the propagating interface stabilizes the grain packing above. Once vibrations perturb the system, the interface becomes disturbed and breaks down before the pressure reaches the non-perturbed value ΔP_{min} . This

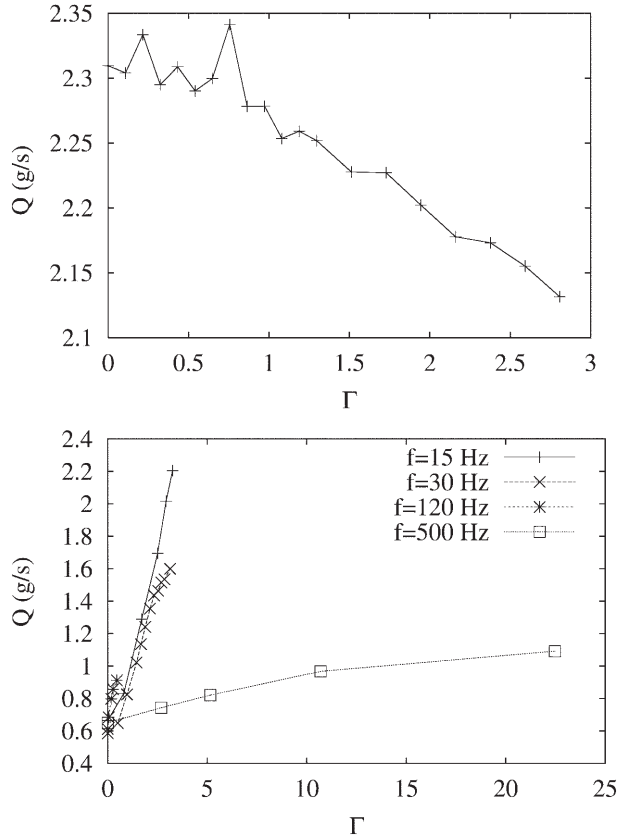


Fig. 15. Top: Flow rate versus Γ for a steady flow (no cork). The grain type is A7 and the vibration frequency is 30 Hz. Bottom: Flow rate versus Γ for a relaxation flow. The results are for A10 grains

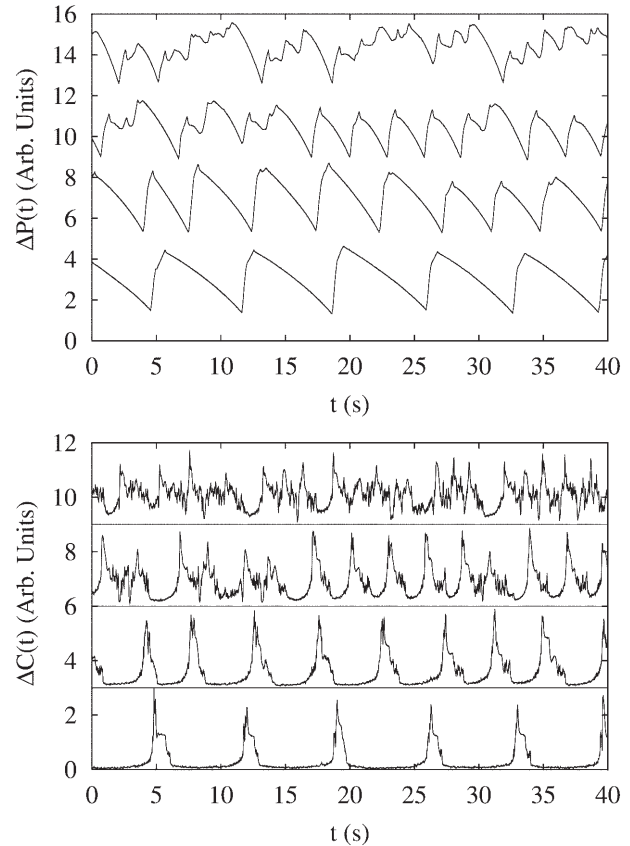


Fig. 16. Pressure (top) and capacitance (bottom) signals of A10 grains. The data are all for $f = 30$ Hz and have been shifted for clarity. From bottom to top: $\Gamma = 0, 1.5, 2.3,$ and 3.1

premature collapse of the interface causes the flow to become more unstable, increasing the average flow rate. This increase leads to a higher average pressure difference and thereby an increasing air flow. Thus the fixed frequency ticking becomes disturbed and the peak disappears. This can also be seen in Fig. 17 where the power spectra of the signals in Fig. 16 are shown. As Γ increases, the peak in the non-vibrated spectrum spreads out and flattens the spectrum. A characteristic time scale is still left as a cutoff in the spectrum. A general feature is that this characteristic time scale moves to higher frequencies as Γ is increased. This is reasonable since the relaxation time τ (see e.g. Eq. (7)) is inversely proportional to the permeability κ . As Γ is increased κ also increases leading to a shorter relaxation time with a correspondingly shorter ticking period.

7

Conclusions

In conclusion, we have found that the relaxation oscillation flow in a gradually narrowing stem of an hourglass will manifest itself with propagating interfaces for sufficiently large grain sizes. For small grains the interfaces were found to be stationary and the pressure relaxation was exponential. We found that the propagation of the interfaces will result in a modification of the air pressure

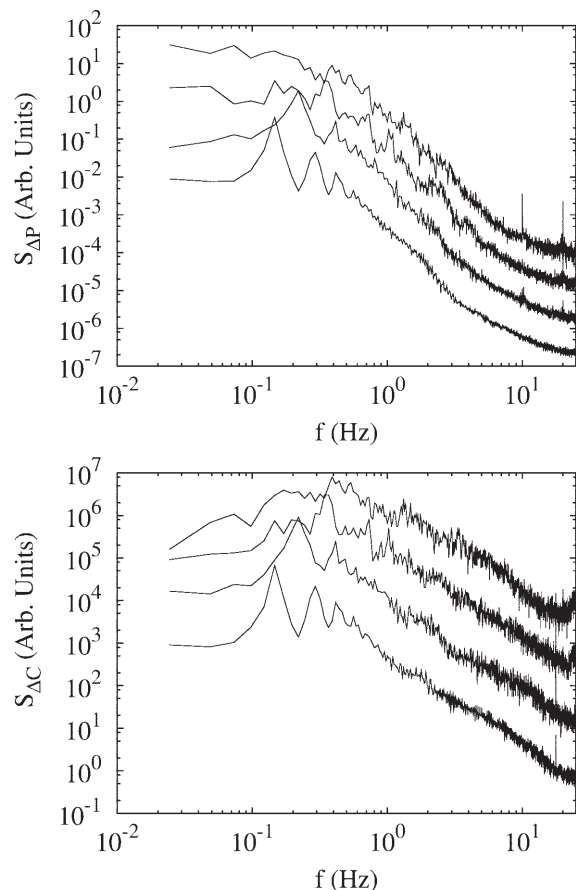


Fig. 17. Power spectra of the pressure and capacitance signals shown in Fig. 16. The data have been shifted for clarity. From bottom to top: $\Gamma = 0, 1.5, 2.3,$ and 3.1

decay. The particular form of the decay is highly dependent on the specific geometry of the outlet. If the geometry is assumed to be a pipe of constant diameter the propagation results in a power-law decay. We have also established pressure conditions for stationary, propagating and collapsing interfaces.

The long time behavior of the oscillation flow shows signs of a non-stationary process. The non-stationarity arises from the gradually emptying reservoir. However, the expected long term behavior for the relaxation time constant was not found to agree with measurements.

External vibrations applied to the system were found to increase the characteristic time constants. This was attributed to a larger permeability of the grain packing induced by the vibrations. Likewise, we found that in the case of relaxation flow the average mass flow rate increased, unlike the steady flow case where the average mass flow rate decreased.

References

1. A. A. Mills, S. Day, & S. Parkes, Mechanics of the sand-glass. *Eur. J. Phys.*, 17 (1996), p. 97
2. H. M. Jaeger, S. R. Nagel, & R. P. Behringer, The physics of granular matter. *Physics Today*, April (1996), p. 32–38
3. H. M. Jaeger, S. R. Nagel, & R. P. Behringer, Granular solids, liquids, and gases. *Reviews of Modern Physics*, 68(4) (1996), p. 1259–1273
4. R. P. Behringer & J. T. Jenkins, editors, *Powders & Grains 97*. Balkema, Rotterdam, 1997
5. H. J. Herrmann, J.-P. Hovi, & S. Luding, editors, *Physics of dry granular media*. Kluwer Academic Publishers, Dordrecht, 1998
6. K. L. Schick & A. A. Verwee, $1/f$ noise with a low frequency white noise limit. *Nature*, 251 (1974), p. 599
7. X. L. Wu, K. J. Måløy, A. Hansen, M. Ammi, & D. Bideau, Why hour glasses tick. *Phys. Rev. Lett.*, 71(9) (1993), p. 1363–1366
8. P. Evesque & W. Meftah, Mean flow of a vertically vibrated hourglass. *Int. J. of Mod. Phys. B*, 7(9 & 10) (1993), p. 1799–1804
9. T. Le Pennec, K. J. Måløy, A. Hansen, & M. Ammi, Ticking hour glasses: Experimental analysis of intermittent flow. *Phys. Rev. E*, 53(2) (1996), p. 2257–2264
10. C. T. Veje & P. Dimon, Power spectra of flow in an hourglass. *Phys. Rev. E*, 56(4) (1997), p. 4376–4380
11. J. O. Cutress & R. F. Pulfer, X-ray investigations of flowing powders. *Powder Tech.*, 1 (1967), p. 213–220
12. J. Lee, S. C. Cowin, & J. S. Templeton, An experimental study of a kinematics of flow through hoppers. *Trans. Soc. Rheol.*, 18 (1974), p. 247
13. R. L. Michalowski, Flow of granular material through a plane hopper. *Powder Techn.*, 39 (1984), p. 29
14. G. W. Baxter, R. P. Behringer, T. Fagert, & G. A. Johnson, Pattern formation in flowing sand. *Phys. Rev. Lett.*, 62(24) (1989), p. 2825
15. C. T. Veje & P. Dimon, Two-dimensional granular flow in a small-angle funnel. *Phys. Rev. E*, 54(4) (1996), p. 4329–4337
16. R. L. Brown & J. C. Richards, *Principles of powder mechanics*. Pergamon Press, 1970
17. S. Hørnlück & P. Dimon, Statistics of shock waves in a two-dimensional granular flow. *Phys. Rev. E*, 60(1) (1999), p. 671–686

18. E. Clément, Private communications
19. T. Pöschel, Recurrent clogging and density waves in granular material flowing through a narrow pipe. *J. Phys. I France*, 4 (1994), p. 499
20. S. Horikawa, T. Isoda, T. Nakayama, A. Nakahara, & M. Matsushita, Self-organized critical density waves of granular particles flowing through a pipe. *Physica A*, 233 (1996), p. 699–708
21. T. Raafat, J. P. Hulin, & H. J. Herrmann, Density waves in dry granular media falling through a vertical pipe. *Phys. Rev. E*, 53 (1996), p. 4345–4355
22. O. Moriyama, N. Kuroiwa, & M. Matsushita, $4/3$ law of granular particles flowing through a vertical pipe. *Phys. Rev. Lett.*, 80(13) (1998), p. 2833–2836
23. A. Nakahara & T. Isoda, $1/f^\alpha$ density fluctuations at the slugging transition point of granular flows through a pipe. *Phys. Rev. E*, 55(4) (1997), p. 4264
24. E. Clément & K. Måløy, Private communications
25. T. Pennec, K. J. Måløy, E. G. Flekkoy, J. C. Messenger, & M. Ammi, Silo hiccups: Dynamic effects of dilatancy in granular flow. *Phys. Fluids*, 10(12) (1998), p. 3072
26. A. Suzuki, H. Takahashi, & T. Tanaka, Behaviour of a particle bed in the field of vibration. ii. flow of particles through slits in the bottom of a vibrating vessel. *Powder Tech.*, 1968
27. M. L. Hunt, R. C. Weathers, A. T. Lee, C. E. Brennen, & C. R. Wassgren, Effects of horizontal vibration on hopper flows of granular materials. *Phys. Fluids*, 11(1) (1999), p. 68–75